



Automated shock detection and analysis algorithm for space weather application

Vasily S. Vorotnikov,¹ Charles W. Smith,² Qiang Hu,³ Adam Szabo,⁴ Ruth M. Skoug,⁵ and Christina M. S. Cohen⁶

Received 17 August 2007; revised 26 November 2007; accepted 21 December 2007; published 13 March 2008.

[1] Space weather applications have grown steadily as real-time data have become increasingly available. Numerous industrial applications have arisen with safeguarding of the power distribution grids being a particular interest. NASA uses short-term and long-term space weather predictions in its launch facilities. Researchers studying ionospheric, auroral, and magnetospheric disturbances use real-time space weather services to determine launch times. Commercial airlines, communication companies, and the military use space weather measurements to manage their resources and activities. As the effects of solar transients upon the Earth's environment and society grow with the increasing complexity of technology, better tools are needed to monitor and evaluate the characteristics of the incoming disturbances. A need is for automated shock detection and analysis methods that are applicable to in situ measurements upstream of the Earth. Such tools can provide advance warning of approaching disturbances that have significant space weather impacts. Knowledge of the shock strength and speed can also provide insight into the nature of the approaching solar transient prior to arrival at the magnetopause. We report on efforts to develop a tool that can find and analyze shocks in interplanetary plasma data without operator intervention. This method will run with sufficient speed to be a practical space weather tool providing useful shock information within 1 min of having the necessary data to ground. The ability to run without human intervention frees space weather operators to perform other vital services. We describe ways of handling upstream data that minimize the frequency of false positive alerts while providing the most complete description of approaching disturbances that is reasonably possible.

Citation: Vorotnikov, V. S., C. W. Smith, Q. Hu, A. Szabo, R. M. Skoug, and C. M. S. Cohen (2008), Automated shock detection and analysis algorithm for space weather application, *Space Weather*, 6, S03002, doi:10.1029/2007SW000358.

1. Introduction

[2] Shocks observed at 1 AU most often form as bow shocks driven by coronal mass ejections (CMEs) [see, e.g., Gosling and Pizzo, 1999, and references therein]. Less often they are seen in association with corotating interaction

regions (CIRs). Very occasionally a reverse shock is observed at 1 AU as part of the forward-reverse shock pair normally expected for CIRs at greater heliocentric distances. Interplanetary shocks and their associated transient drivers have geomagnetic effects for four basic reasons: (1) They constitute a propagating density compression ahead of the driver gas that impacts the outer boundary of the magnetosphere [Boyd and Sanderson, 1969], (2) The propagating compression is responsible for the acceleration of energetic particles which may enter the magnetosphere either by way of the polar regions or via reconnection [Lee, 1984; Forman and Webb, 1985; Thomsen, 1985; Armstrong et al., 1985; Desai et al., 2003; Kress et al., 2005], (3) Shocks mark the outer boundary of the sheath region of turbulent flow upstream of the ejecta which can itself have a strong perturbative effect on the magnetospheric boundary [Gosling and McComas, 1987; Siscoe et al., 2007], and (4) Shocks serve as a precursor for the pending arrival of the

¹Department of Chemical Engineering, University of New Hampshire, Durham, New Hampshire, USA.

²Space Science Center, University of New Hampshire, Durham, New Hampshire, USA.

³Institute of Geophysics and Planetary Physics, University of California, Riverside, California, USA.

⁴NASA Goddard Space Flight Center, Greenbelt, Maryland, USA.

⁵Los Alamos National Laboratory, Los Alamos, New Mexico, USA.

⁶Space Radiation Laboratory, California Institute of Technology, Pasadena, California, USA.

driver gas which often contains a magnetic flux rope that can have strong southward IMF components and geomagnetic effects [Burlaga, 1995; Webb, 2004; Kappenman, 2005].

[3] It seems that in some instances the effect of the shock can be isolated and studied independent of the rest of the disturbance [Echer *et al.*, 2006]. The presence of a shock and a strong driver disturbance act in concert to drive perturbations in the magnetospheric currents and radiation belts [Hudson *et al.*, 1995, 1997]. Echer and Gonzalez, [2004] argue that 22% of all interplanetary shocks are intensely geoeffective while 35% are moderately geoeffective. When acting in concert with magnetic clouds, those numbers become 43% and 38%, respectively. They also state, "Mechanisms associated to shock geoeffectiveness are well known, such as the compressed/shock fields in the sheath region. It is also known that faster ejecta, which are more likely to drive shocks, have higher magnetic field intensity and are potentially more geoeffective [Gonzalez *et al.*, 1999]." This points to strong shocks providing the greatest geoeffective response. However, at solar active times a second ejecta may encounter the Earth before the effects of the first ejecta have subsided to produce compound effects in the magnetosphere [Farrugia *et al.*, 2006]. Therefore, it seems useful that we have a space weather tool that can identify, isolate, and analyze interplanetary shocks in real time to work in concert with in situ measurements of the energetic particles [Vandegriff *et al.*, 2005; Posner, 2007] and ejecta to provide useful space weather information prior to the disturbance's arrival at Earth. Attempts to model the Sun-to-ground evolution and the effects of solar transients, especially compound events, reveal that much remains to be done in predicting the characteristics of the disturbance upon arrival at Earth [Xie *et al.*, 2006; Tóth *et al.*, 2007; Trichtchenko *et al.*, 2007; Dryer *et al.*, 2004; McKenna-Lawlor *et al.*, 2006] and so real-time evaluation of the disturbance before arrival at Earth allows for correction of any long-term predictions that originate from observations closer to the Sun. The Advanced Composition Explorer (ACE) working together with the NOAA/SEL facility already provides real-time data for thermal plasma, fields, and energetic particle measurements [Zwickl *et al.*, 1999]. The analysis method we describe here can use this data to identify and analyze the shocks that pass the spacecraft ~ 1 h prior to encounter with the Earth's magnetosphere. We will find below that the method described here fails to find weak shocks to any reliable degree, but we note above that strong shocks provide the most geoeffective drivers and will content ourselves with the ability to recognize, capture, and analyze strong shocks as a good starting point for this contribution to space weather efforts.

[4] We describe a method for performing an automated shock analysis that can run without operator intervention to provide useful predictive ability for shock parameters prior to the shock's arrival at Earth. Those parameters include, but are not limited to, magnetopause arrival times as well as shock strength and geometry. The code is

presently configured for space weather applications to identify shock passages and compute the shock solutions automatically with as few false positives as is possible subject to the constraint of trying to maximize the number of real shock identifications. It is possible to run in a different configuration that will permit the scanning of established data sets to yield a maximum number of shock solutions without regard for false positive events, but in this application we run it in a space weather mode where false positive solutions can be problematic. The analysis can be tuned as desired to provide maximum performance for any application. It is important to note that we use a popular and well-proven shock solution method in this analysis. However, our purpose is to demonstrate how shocks may be found in the data, analyzed, and reliably reported in space weather environments. A key aspect of this is the ability to discard disturbances that are not true shocks. Any algorithm that yields a reliably complete set of shock parameters may be substituted for the shock solution method we describe below.

2. Shock Equations

[5] The shock analysis used here is based on the Rankine-Hugoniot (R-H) jump conditions that derive from basic conservation relations for isotropic plasmas. Using subscripts n and t to denote the normal and tangential components of vectors relative to the shock surface (assumed to be locally planar), we can write [Boyd and Sanderson, 1969]:

$$\Delta[\rho V_n] = 0 \quad (1)$$

$$\Delta\left[\rho V_n^2 + P + \frac{B^2}{8\pi}\right] = 0 \quad (2)$$

$$\Delta\left[\rho V_n V_t - \frac{B_n B_t}{4\pi}\right] = 0 \quad (3)$$

$$\Delta\left[\left(\frac{1}{2}\rho V^2 + \frac{5}{2}P + \frac{B_t^2}{4\pi}\right)V_n - \frac{B_n B_t}{4\pi}V_t\right] = 0 \quad (4)$$

$$\Delta[B_n] = 0 \quad (5)$$

$$\Delta[(\mathbf{n} \times \mathbf{V}_t)B_n - (\mathbf{n} \times \mathbf{B}_t)V_n] = 0 \quad (6)$$

where Δ represents the difference across the boundary, ρ is the mass density of the plasma, \mathbf{V} is the solar wind velocity, \mathbf{B} is the IMF vector, P is the plasma pressure, and \mathbf{n} is the shock normal. Equations (1)–(6) represent conservation of mass, normal momentum, tangential momentum, energy flux, magnetic normal component,

and tangential electric field, respectively. These equations hold in the shock frame of reference and the energy flux equation assumes $\gamma = 5/3$.

[6] From the solutions to equations (1)–(5) we obtain the shock normal, shock velocity in the plasma frame V_P , shock velocity in the spacecraft frame $V_S = V + V_P$, Alfvén Mach number $M_A = V_P/V_A$ where V_A is the Alfvén speed, mass flux through the shock surface ρV_P , and downstream over upstream density and magnetic field compression ratios $R_N = \rho_{down}/\rho_{up}$ and $R_B = |B|_{down}/|B|_{up}$. Shock speed and direction of propagation serve as predictors of shock arrival time at the Earth’s magnetopause. Mach number and compression ratios predict how strong the shock will be at arrival. The solutions to the above equations can be used to distinguish between the forms of discontinuity, including shock, observed by the spacecraft. The same equations can also be used to find solutions to other discontinuities (contact, rotational, and tangential). However, the current version analyzes only shocks. Modifications to the program may yield other desired information.

[7] We solve a reduced set of these equations by ignoring equations (2) and (4) and thereby obtaining solutions without the need for temperature data. We use a method that was originally developed by *Viñas and Scudder* [1986] and then further improved by *Szabo* [1994]. This technique employs a two-dimensional nonlinear least-squares analysis of the R-H jump conditions leading to an optimal solution for the shock normal for the points chosen to represent the upstream and downstream conditions. Omitting the temperature data may sometimes result in a second spurious solution, but it has the benefit of being applicable to real-time data where electron temperatures are unavailable. From this nonlinear least squares fitting the shock speed is obtained and the remainder of the shock jump conditions are evaluated. These mappings are useful to the interactive user in determining whether the best solution is significantly better than all other solutions. Although guided by rigorous analysis, determination of whether the nonlinear least squares fitting is unacceptable is part of a highly subjective process and can lead the user to select different upstream or downstream points. The interactive code also has a tendency to run into an infinite loop jumping between two widely spread solutions. Owing to this infinite loop problem and the subjectivity of the process, the automated code uses an alternate means of dealing with data point selection that we describe below.

[8] The adapted interactive code performs an asymptotic states analysis from the best fit jump conditions, shock normal, and shock speed to obtain upstream and downstream values for the fields with their uncertainties. These values are expressed in terms of the density, and hence accurate density measurements are a crucial requirement in this analysis and data point selection.

3. Automated Analysis Technique

[9] As *Kallenrode* [2001, p. 145] observes, interplanetary shocks can have “. . . [density] compression ratio between 1

and 8 with an average close to 2. . . magnetic compression [ratio]. . . with an average at 1.9. . . Alfvén Mach number is between 1 and 13 with an average at 1.7.” While it is possible to observe very strong interplanetary shocks, as these values indicate most shocks are relatively weak. An analysis of all shocks observed by the Wind spacecraft from 1994 to 1997 confirms that weak shocks with low Mach number constitute the most common observation [*Berdichevsky et al.*, 2000]. This is the foremost complication in developing an automated analysis: keeping as many real shocks while discarding events with nearly comparable compression ratios that are, in fact, not shocks at all. There is little value to a space weather product that “cries wolf” too often. We can configure the algorithm to reject most false positive shock candidates; however, the price we pay for this reliability is that the weakest real shocks (that have the least impact on space weather) are often omitted as well. So long as space weather interests continue to focus on the strongest shocks exclusively, this trade-off is acceptable.

[10] The automated detection and analysis of shocks in interplanetary data is a seven-step process. The first three steps involve finding likely shock candidates and selecting upstream and downstream data for the analysis. The next two (steps 4 and 5 below) involve the fitting of the data to the R-H jump conditions to obtain a solution that includes propagation speed, its direction, density, and magnetic compression. We use the methods of *Viñas and Scudder* [1986] and *Szabo* [1994] to obtain solutions to the shock equations, but the technique described here is applicable to any method that yields valid shock parameters. The remaining two steps of the analysis are normally performed in some comparable manner by the operator. They involve passing judgment on the quality of the solution. When the solution obtained in this manner is judged to be unacceptable, the investigator will either judge the interval to be something other than a shock or select other upstream and downstream points to represent the plasma conditions. The automated analysis must perform these steps in a reasonable manner so as to produce results in good agreement with the best interactive solutions while reliably determining whether the candidate event is, in fact, a shock or is possibly something else to be discarded or noted differently.

[11] We developed and tested the code in a manner that closely resembles the anticipated real-time application. We used science-quality Level-2 data from the Advanced Composition Explorer (ACE) mission [*Stone et al.*, 1998] that merges thermal ion data from the SWEPAM instrument [*McComas et al.*, 1998] with magnetic field data [*Smith et al.*, 1998]. We did this because many of these shocks have been already analyzed and comparison can be made against the best interactive solutions. The data files contain date, time, proton density, temperature, bulk speed, three components of the solar wind velocity in RTN coordinates, three components of average interplanetary magnetic field (IMF) also in RTN coordinates, and the

average IMF scalar magnitude. Data are recorded every 64 s and handled in a manner that closely resembles the 1-min environment of the NOAA real-time data stream.

3.1. Step 1: Identify Shock Candidates

[12] The first step in analyzing a shock is finding a suitable candidate. A shock finding subroutine compares each of two consecutive data points (or with a gap of one point in case of missing data) and looks for jumps in velocity, temperature, and proton density. SWEPAM has a missing data point every half hour to accommodate download of an additional data product. Too many sequential data gaps obscure the shock identification and this implementation does not look across data gaps larger than 1 point. The least constrained values for finding these jumps based on the weakest shocks manually found in the 1999 ACE data include 1.5% jump in velocity, 15% jump in temperature, and 20% jump in proton density. By selecting only those candidates with combined percentage values >68, a significant number of false shock candidates can be eliminated prior to analysis using the shock jump conditions. These values are easy to adjust by the user depending on what strength shocks he/she might want to find. There are advantages and disadvantages to adjusting these values which are discussed below.

3.2. Step 2: Refining Shock Candidates

[13] To improve the shock-finding code, the averages of velocity, temperature, and density are used as a second shock test. Ten data points immediately before and 10 data points after the shock candidate time are selected and bad data with fill value is disregarded so that fewer than 10 points may sometimes be considered. With ACE/SWEPAM data resolution at 64 s, this translates into an examination of the data just under 11 min either side of the shock. Examining the wind speed, density, and temperature separately, we select three points from before and after the shock that are not necessarily consecutive but are closest in value and average the values on either side of the discontinuity. The three points chosen for one parameter may not be the same points chosen for another. In this way we obtain new values for the average upstream and downstream plasma parameters and apply the same shock jump test as above. This second test proves to be useful in eliminating false positive shock candidates that were previously based on a single pairing of sequential data values because it removes short-term fluctuations in the data. Focusing on ACE data from 1999 alone, this single second step in the shock finding algorithm keeps all the shocks previously analyzed interactively while eliminating 705 false positives. This reduces the number of shock candidates to be further analyzed from 1022 to 317 in the 1999 data set.

3.3. Step 3: Select Upstream and Downstream Data Points

[14] Although separately comparing wind speed, density, and temperature jumps is useful in rejecting many

false positive shock candidates, the final shock solutions must be based on a common selection of points for all variables. Because the wind speed can vary greatly and independently from the shock speeds, we use the data points from the density selection in step 2, together with all variables from those data times, as input for our shock solutions. These are the points with the most closely grouped density values before and after the shock. Such density-dependent picks allow for better solutions, and better agreement with the interactive solutions, as determined from running the 2000 ACE data. These are the points (three points upstream and three downstream) which are passed to the shock solving algorithm for analysis of the R-H equations.

3.4. Step 4: Obtain Shock Normal and Speed

[15] The set of shock equations is projected into the parameter space (θ, ϕ) , the angular direction of the normal of a planar shock. A nonlinear least squares formula of variables, θ and ϕ , is constructed to represent the least squares minimization of deviations, χ^2 , between the theoretically predicted values and actual in situ spacecraft measurements, taking into account uncertainties associated with each individual data points [Viñas and Scudder, 1986; Szabo, 1994]. A standard least squares minimization algorithm is employed to find the optimal solution, the pair of (θ, ϕ) that corresponds to minimum χ^2 , thus giving the best-fit shock normal based on the R-H relations and the observational data. The uniqueness and goodness of the solution are evaluated by the standard χ^2 map over the entire (θ, ϕ) parameter space and the χ^2 statistics [Szabo, 1994].

[16] The algorithm involves an iteration procedure starting from an initial guess of (θ, ϕ) , and often the initial guess is crucial to ensuring the convergence of the solution. A well-educated guess comes from an extra step in which iterations are carried out for selected (θ, ϕ) parameters over a finite two-dimensional (2-D) grid spanning the whole parameter space. Each yields a χ^2 value. Then a pair of (θ, ϕ) that is close to the one of minimum χ^2 is used as the initial guess to start the iteration to converge to the best-fit solution. In the case of multiple local minima, it is necessary to repeat the iteration and the following shock-diagnostic steps for each corresponding pair of (θ, ϕ) to determine a best-fit shock solution.

[17] An upper limit on the number of total iterations allowed has to be set to avoid the occasional infinite loop. Although we expect most cases to converge within a few iterations, failure of convergence can occur. In concept, the best remedy is either to start from another initial guess, especially when multiple minima appear on the χ^2 map, or to simply return to step 3 to select a different set of upstream and downstream data points. In our automated analyses we choose, instead, to treat the shock candidate as poor and reject it from further consideration. The few

candidates rejected in this manner for the years 1999–2005 do not appear to be real shocks. Once the shock normal is obtained, equation (1) provides the shock speed using the observed upstream and downstream plasma velocity and density data.

3.5. Step 5: Obtain Asymptotic Magnetofluid State

[18] The next step is to obtain the R-H conservation constants and to calculate the self-consistent asymptotic magnetofluid states upstream and downstream of the shock. Again, these involve a one-dimensional nonlinear least squares procedure that minimizes a system of functions of a single variable, ρ , the mass density, by applying the same algorithm as in step 4. Once the optimal conservation constants and the mass density are determined for both upstream and downstream of the shock, the asymptotic magnetofluid states, \mathbf{V} , \mathbf{B} , and thermal pressure jump, ΔP , are obtained as well. Consequently, the downstream over upstream compression ratios of magnetic field, R_B , and density R_N , are calculated from these asymptotic values in addition to direct calculation using downstream and upstream averages.

3.6. Step 6: Judge the Quality of the Solutions

[19] The sixth step is to discard false positive events based on the candidate's asymptotic solution to the R-H equations. In principle, the continuity relations that form the R-H equations should hold everywhere in space where there is no surface charge (such as the side of a spacecraft that exhibits charging), but the value of the conserved quantities will generally be small. For instance, mass flux in the plasma frame at any given location in space may be conserved but will generally be small. Conservation of the R-H quantities is one good indicator of the quality of the shock solution. However, use of the R-H equations to separate true from false shock candidates must be based not on how well the quantities are conserved but how far from zero they are statistically. As presently configured, the test accepts shock candidates if $M_A > 0.7$ (most real shocks have a higher Mach number), $V_S/\sigma_{VS} > 2.9$ where σ_{VS} is the uncertainty in the computed shock speed, $\rho V_P/\sigma_{\rho VP} > 3.0$, and the tangential momentum divided by its uncertainty is greater than 0.5. This same test could be reformulated using the same or similar shock quantities such as normal magnetic field, tangential electric field, or shock normal (asymptotic solution); however, our attempts with other formulations pass many false positives and are not described further.

[20] These values are chosen because they will admit moderate to strong shocks while rejecting most false positives. The false positives that pass this test tend to be weak. Real shocks that fail tend to be similarly weak and not of great importance to space weather applications. Some real shocks do not pass the shock solver conditions for several reasons. Some shocks are rejected prior to analysis due to missing temperature or other proton data.

This is either the result of high radiation levels that can occur upstream of some shocks or the presence of a low wind speed when the SWEPAM instrument struggles. Since the shock speed is a critical part of space weather applications, and since this can not be obtained without thermal proton data, these shocks are not analyzed by this method and are passed over in the first step of the analysis.

3.7. Step 7: Rank by Shock Solution Quality

[21] While we find that the above shock test performs reasonably well, we will show below that it tends to admit too many false positive solutions and too many poor solutions for reliable space weather applications. We therefore apply one final step in shock analysis designed to remove false positives previously accepted while keeping the strongest of the shocks. We make sure that the shocks accepted are indeed strong shocks (those of high interest to space weather applications) with self-consistent solutions by assigning points to each aspect of the shock solution. To do this we create a point system to evaluate the quality of the solution and the strength of the shock and use this in a final pass/fail analysis. The details will be described below.

3.8. Analysis Run Times

[22] Step 4 (the nonlinear least-squares fitting) is the most time-consuming part of the analysis. For this reason, the shock finding algorithm has evolved to reject as many false positives as possible with simple point-to-point comparison and only then run the shock fitting subroutines after which additional false positives are discarded using the conservation equations. Although the code was developed on a 400 MHz VMS workstation where each shock candidate required 4:50 min to analyze, now running on a 3 GHz Intel Dual Core processor the code requires only 7.3 s to compute a shock solution. The entire 1999–2000 data set, with a total of 658 shock candidates, can be processed with solutions in under 40 min and the entire 10-year ACE data set can be run in 6 h. New solutions for previously unanalyzed shocks will soon be available at the ACE web site. Since the real-time data has 1 min cadence, it will be a simple matter for the analysis to stay ahead of the data during even the most active phase of the solar cycle. The greatest delay will come from having to obtain a sufficient number of downstream data values to process a good solution. Efforts are underway to experiment with using only a single downstream point to analyze the strongest shocks.

4. Results

[23] We tested the automated shock algorithm on 4 years of ACE Level-2 data from 1999–2002. We limited the test to these years because they have the greatest number of interactive shock analyses against which to test the automated analysis. For the purposes of demonstration, we omit step 7 until later. Table 1 contains statistics

Table 1. Automated Shock Finding Performance Statistics 1999–2002

	Real Shocks	False Positives
Shocks Identified by MAG/SWEPAM Team	243	0
Interactive solutions	163	0
Shocksolver after step 1	177	3893
Shocksolver after step 2	161	949
Shocksolver after step 6	102	31
Both Interactive and Automated Solutions	98	0

on the code’s performance including the number of shocks found in step 1 and then step-by-step the ability of the code to reject false positive candidates and retain real shocks. The shock finder found 177 out of 243 real shocks in the data interval. The input selection conditions could be changed to find more of the real shocks, but this also means admitting more false positives. In step 6 the code retained 102 out of 243 real shocks with 98 of these having interactive solutions. This means that 98 out of the 163 total interactive solutions were analyzed and compared. The number of false positives was reduced to 31 from an initial value of 3893. This is the step that is most crucial to this work, the selective elimination of false positive shock candidates. Other shock codes exist and can be automated, and in time we can develop better ways of finding shock candidates in the data, but the ability to reject false positives so that a space weather application does not “cry wolf” too often is the crucial objective of this analysis.

[24] Table 2 lists the statistics on the strongest shocks in the ACE data set during these years with the number in parentheses listing the count of events that meet the criterion by better than 1σ . The strongest shocks have the most significant space weather impacts. Statistics for real shocks found and missed are based on the ability of the automated code to find events solved by interactive analysis. For instance, the automated code missed 10 shocks with interactive solutions $M_A > 3$, but only three had $M_A > 3$ to better than one standard deviation. So it is true that the automated analysis still misses some strong shock events in spite of our best efforts. Statistics for false shocks found are based on the values from the automated solutions. We define a strong shock to have either $M_A > 3$, $R_N > 3$, or $R_B > 3$. Only one false shock was identified with $M_A > 3$ and no false shocks met this condition by better than 1σ . Although the statistics are gathered separately for the three conditions, there is strong overlap between the rows (for instance, $M_A > 3$ missed and $R_N > 3$ missed contain many of the same events). The automated analysis finds more than two thirds of the strong shocks by these definitions while passing a total of three false positive identifications. Two of the three false positive solutions are based on values of $R_B > 3$ that have large uncertainties in the automated solutions, are poor solutions, and are not $R_B > 3$ solutions in the statistically significant sense. In a real-time application these

solutions would most likely be discarded. This points to a possible refinement of the method that discounts solutions with large uncertainties and further exploration of this code will enable us to set a functional limit for tolerable uncertainties. However, one of the two R_B events may be a shock of weaker density compression ($R_N = 1.4$) not previously identified by the ACE team due to local variation in the measured parameters. The $M_A = 3.1 \pm 0.8$ event listed as a false shock in Table 2 may actually be a previously unidentified shock with $M_A \sim 2$ that was discredited earlier due to large variations in proton temperature around the time of the shock. Again, the automated solution does not yield $M_A > 3$ in a statistically significant sense.

[25] Examination of the real shocks missing from the automated analysis as listed in Table 2 yields equally interesting insights into the nature and variability of interplanetary shocks. For instance, two previously identified shocks on day 234 of 1999 and day 118 of 2001 show delayed density jumps 1 min after the coincident velocity, temperature, and magnetic field intensity jumps. The ACE teams have identified these events to be real shocks with some transient complications. The automated analysis is unable to make this judgement. The code could be adapted to look for broader jumps in solar wind parameters, but this would admit a great many more false positive solutions. It is important to understand that only a fraction of interplanetary shocks manifest as textbook examples of propagating discontinuities. Many shock observations are complicated by ramping background parameters, local structures, and various transient features that make reliable shock identification a nonlocal judgement that is beyond the scope of this analysis. Complicating features such as the above often lead to poor solutions even in the interactive analysis. For instance, of the 10 missed shocks with $M_A > 3$ in the interactive solutions only three have computed uncertainties that place $M_A > 3$ with statistical significance. Only two of the 10 events with interactive solutions $R_N > 3$ are statistically significant. Only one of the five events with interactive solutions $R_B > 3$ are statistically significant. The overlap in the above list of strong events missed is such that there are only five real shocks missed in this analysis with one or more of the above conditions ($M_A > 3$, $R_N > 3$, or $R_B > 3$). These numbers are represented by parentheses in the “Real Missed” column of Table 2. The shock code is therefore subject for further exploration and improvement with respect to more complicated shock scenarios, but overall comparison with

Table 2. Strong Shock Statistics

	Real Missed	Real Found	False Found
$M_A > 3$	10 (3)	26 (14)	1 (0)
$R_N > 3$	10 (3)	13 (7)	0 (0)
$R_B > 3$	5 (1)	9 (2)	2 (0)
$M_A > 3$ or $R_N > 3$ or $M_A > 3$	17 (5)	44 (24)	3 (0)

strong shocks found by the interactive method suggests that the automated shock solutions are close to if not just as good as the interactive solutions.

[26] Of those shocks found by the automated solution with interactive values in the strong shock range, roughly half of the automated solutions for $M_A > 3$ and $R_N > 3$ are within 1σ of the interactive values (where σ is the uncertainty returned from the interactive analysis). The number of automated shock solutions in the strong shock range are listed in Table 2. The number of automated shock solutions that are more than 1σ into the strong shock range are listed in parentheses. Only two of the strong shocks found have $R_B > 3$ at greater than the 1σ level. Of those shocks found by the automated solution but ignored by the interactive analysis, no automated solutions for $M_A > 3$, $R_N > 3$ and $R_B > 3$ are within 1σ of the automated values. These numbers (all zeroes) are represented by parentheses in the “False Found” column of Table 2. The bottom row in Table 2 lists the number of shocks with either $M_A > 3$, $R_N > 3$, or $R_B > 3$.

[27] Figure 1 shows a detailed comparison of the shock speed in the plasma frame for the 98 shocks with both automated and interactive solutions. There is a strong clustering of solutions about the line showing equality between the interactive and automated methods. Uncertainties tend to be tolerably small with most solutions only 1σ off the line. This quantity is important to predicting particle acceleration rates at the shock. Computation of the shock speed in the plasma frame is the first step in predicting the shock arrival time at the Earth’s magnetopause. The comparison shown in Figure 1 suggests good predictions for shock arrival times.

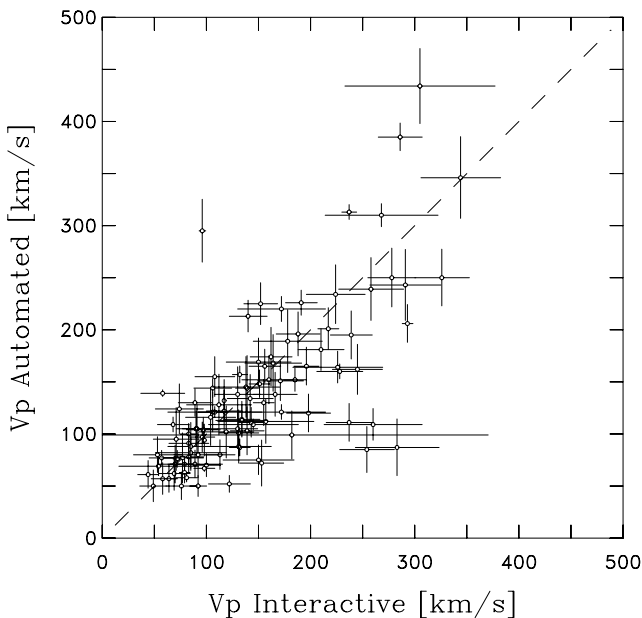


Figure 1. Comparison of automated and interactive analyses of shock speeds in plasma frame, V_p .

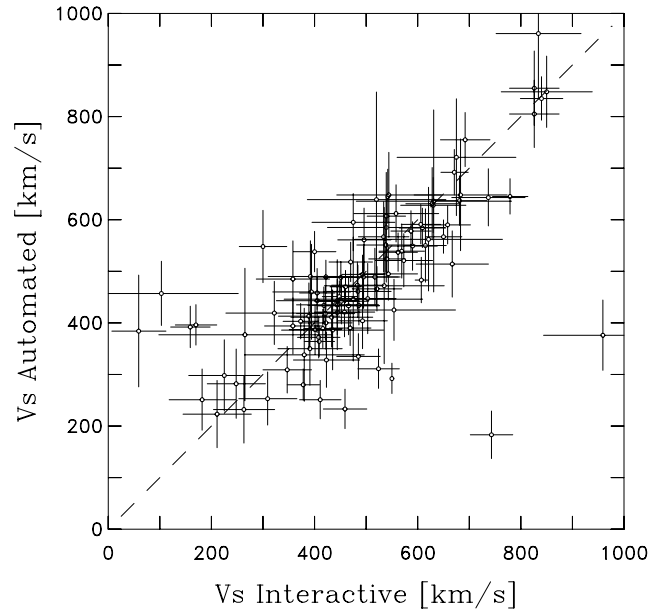


Figure 2. Comparison of automated and interactive analysis of shock speeds in spacecraft frame, V_s .

[28] Figure 2 shows a comparison of the shock speed in the spacecraft frame for the same 98 shocks. Since this folds in the solar wind speed and shock normal, which are computed with the same automated analysis using points selected by the code, additional variation between interactive and automated solutions is possible. Still, the

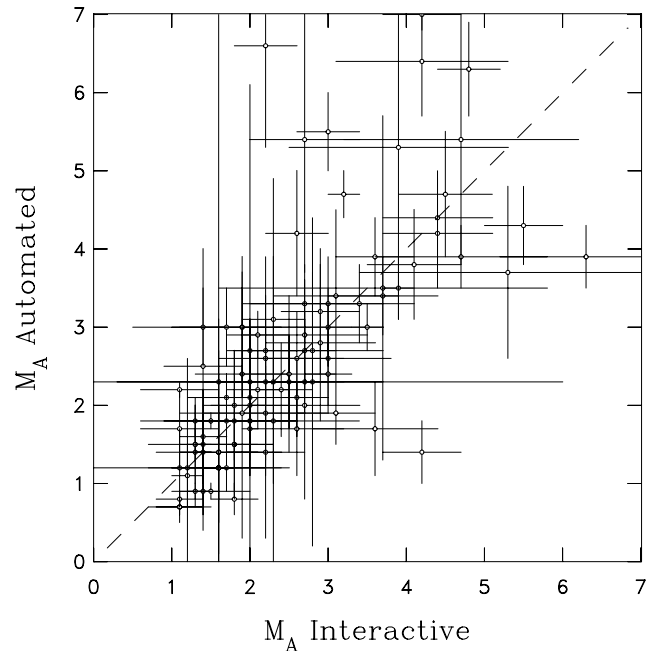


Figure 3. Comparison of automated and interactive analysis of shock speed Mach numbers, M_A .

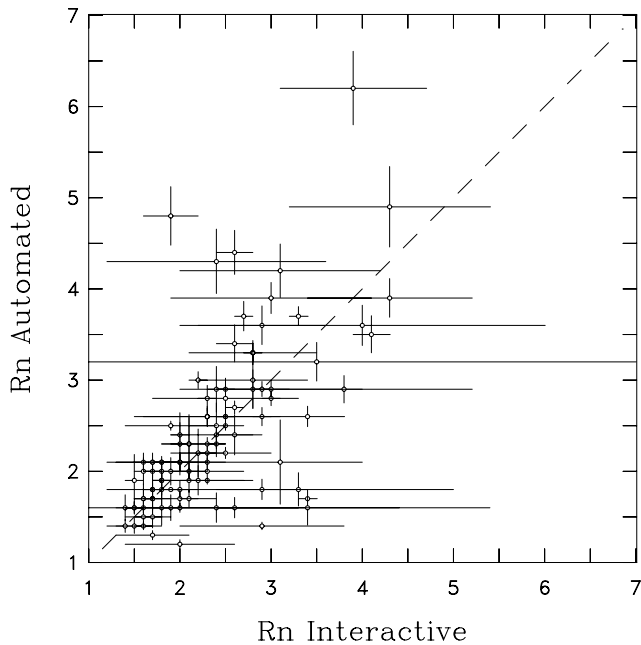


Figure 4. Comparison of automated and interactive analysis of shock density compression ratios, R_n .

agreement is good with only a few solutions more than 1σ off the line.

[29] Figure 3 shows the comparison between interactive and automated values of M_A . The uncertainties are now larger in the relative sense than for the above quantities. This is equally true of the interactive solutions which possess relatively large uncertainties. Still, most solution pairs cluster along the line and are in good agreement. A few solution pairs possess large uncertainties making them relatively useless in any applications. These large uncertainties are generally the result of transient downstream conditions of the type discussed above.

[30] Figure 4 shows the comparison between interactive and automated values of R_n . Note the large uncertainties associated with interactive solutions at large values. This again reflects the difficulty of obtaining reliable solutions when large fluctuations and trends are present in the data. However, the automated solutions are often better defined with smaller uncertainties than the interactive solutions. This is undoubtedly due to the code change that allows three nonconsecutive points to be used in the upstream and downstream regions where the interactive code requires consecutive points. This is just one difference in the philosophy of shock analysis methods that is subject to debate. The choice made here seems to benefit the automated analysis. It is also true that we base the automated point selection of step 3 on density measurements which we hope should enhance the accuracy of the computed density compression ratio. The small variations between automated and interactive solutions shown in Table 4 supports this assertion.

[31] Figure 5 shows the comparison between interactive and automated values of R_B . Since R_B is solely the product of the shock fit and not considered in selecting upstream or downstream points for analysis, it is not surprising that this has large uncertainties in both automated and interactive solutions. Still, the solutions cluster around the line. The relatively close clustering of solutions when compared with uncertainties suggests that the analysis may overestimate the real uncertainty in R_B , but it is not clear at this time why.

[32] Figure 6 shows the comparison between interactive and automated values of Θ_{Bn} . Most solutions are within 1σ of the line, but uncertainties are large in both the interactive and automated solutions. The shock normal direction is one of the most difficult shock parameters to determine and is third in the list of parameters that dictate the shock arrival time at Earth (in addition to the wind speed and V_p). Clearly, the shock normal is the greatest source of error in that computation. The shock normal is also fundamental to theories of particle acceleration by shocks [Jokipii, 1987; Giacalone, 2005] and is necessary to better relate the shock solutions to the observed energetic particle population. Figure 6 also shows what has now been openly discussed: most shocks observed at 1 AU are quasi-perpendicular rather than quasi-parallel [Berdichevsky et al., 2000].

[33] We can provide a statistical comparison of the solutions for any parameter that we select. If for each shock i there is a value for the selected parameter and uncertainty derived by the interactive solution $I_i \pm \sigma_{I,i}$ and for the automated solution $A_i \pm \sigma_{A,i}$ we can com-

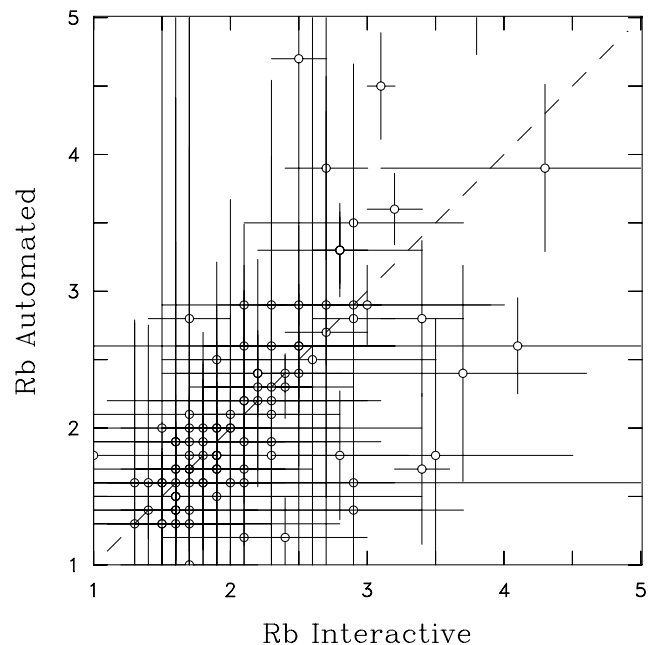


Figure 5. Comparison of automated and interactive analysis of shock magnetic field compression ratios, R_b .

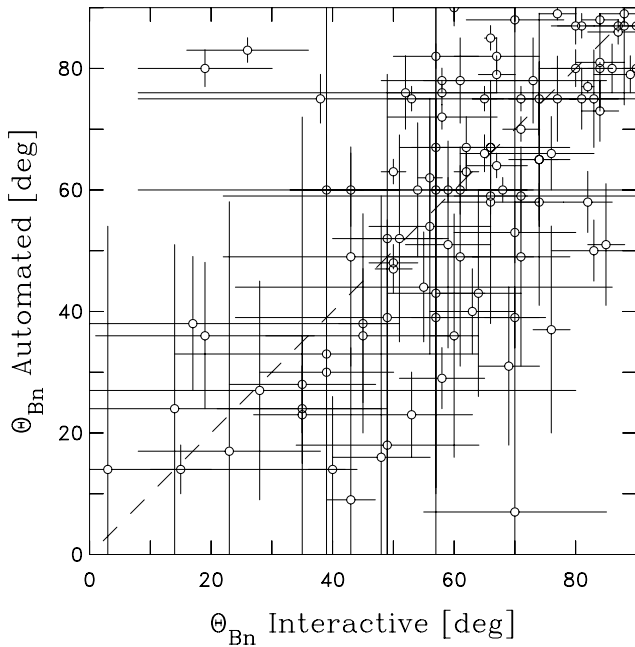


Figure 6. Comparison of automated and interactive analysis of shock normal angles, Θ_{Bn} .

pute a mean difference weighted by the uncertainties according to:

$$\langle |I_i - A_i| \rangle \equiv \left[\sum_i \frac{|I_i - A_i|}{\sigma_{I,i}^2 + \sigma_{A,i}^2} \right] \cdot \left[\sum_i \frac{1}{\sigma_{I,i}^2 + \sigma_{A,i}^2} \right]^{-1} \quad (7)$$

so that a value of $\langle |I_i - A_i| \rangle$ corresponds to a ensemble average of the variance-weighted difference between the interactive and automated analyses. Table 4 gives the results of this comparison. In the interest of identifying shocks with the strongest space weather impact, we can limit the analysis to those shocks with $M_A \geq 3$. Thirty-four shocks meet this condition and their statistics are also listed. Average difference between the interactive and automated solutions is $\Delta M_A \sim 1$, the difference in compression ratios is $\Delta \sim 0.3$, and the difference in shock normal direction is $\Delta \Theta_{Bn} \sim 10^\circ$. The average differences are smaller for weaker shocks suggesting applicability of a fractional error. Although it is desirable to obtain a more accurate and reliable value of M_A , both the automated and the interactive solutions have significant uncertainties made more apparent when one considers the subjective nature of data point selection upstream and downstream of the shock. In addition, most physical problems of interest would benefit from a knowledge of the shock conditions over a broad range of locals across the shock surface. For these reasons, it is doubtful that any shock solution should be trusted to better than

these uncertainties. Textbook shocks are rare in the data and there is growing evidence that the application of planar shock theory to observations at 1 AU can omit important physics [Neugebauer and Giacalone, 2005; Neugebauer et al., 2006].

4.1. Rank by Shock Solution Quality

[34] As we have now demonstrated, the automated solutions using steps 1–6 provide a fairly good environment for running space weather applications, but there are situations where the code misidentifies a false shock solution. In space weather applications the goal is to recognize the strongest shocks while reporting as few false shock warnings as possible. The automated shock code outputs enough information for the user to determine whether the shock is strong. All shock candidates that pass step 6 are real shocks if $V_S/\sigma_{VS} > 14$, $\sigma_{\Theta_{Bn}} < 1.7$, $M_A - \sigma_{MA} > 4.2$, $R_N - \sigma_{RN} > 2.9$, $R_B - \sigma_{RB} > 1.9$, or $\sigma_{VS} < 35$. Adding a test based on these statistics will give us only real shocks and no false positives for the 1999–2005 time period. As a final pass/fail determination of the shock solution we have devised a point system to assess the quality of the solution and gauge whether it should be included as a space weather event. Table 3 lists the point system used in this final step where the shock solution's ability to obtain statistically significant values for eight quantities is examined and the individual point values summed. Figure 7 shows the distribution of point values for all shocks found from late 1998 through early 2005 according to all true shocks and false positives. A real shock solution with a large uncertainty in computed parameters would not be of good use to space weather and for this reason the point system uses not only the computed shock parameters, but also their uncertainties. There is good agreement between the identification of strong shocks via the automated analysis using this shock point system and the interactive solutions. Most strong shocks have higher-value points (above 30), and only one strong real shock with $M_A > 3$ has a point value below 30 (this one event has $M_A < 4$, $R_N < 3$, and $R_B < 3$). Setting a benchmark for accepting shock candidates as real shocks at 30 points will result in 89 real shocks (with 26 of the known 31 strong shocks) while accepting only 5 false positive events in 7 years of data, rejecting 58 false positives along with 54 weak real shocks. Four of the five strong shocks rejected are missed by steps 1 and 2 due to the inability to find the shock and only 1 is rejected due to the quality of the solution. Setting a benchmark for shock candidates at 60 points results in 45 real shocks passing (with 21 of the known 31 strong shocks) with no false positive events. This shock point system proves itself as one of the better shock-finding tools for space weather application due to its selection of good solutions and strong shocks. In a space weather environment this point system could allow the user to still see the shocks previously accepted with an overview provided by the point formula and therefore need not eliminate any real shocks. The point system can be modified with simple

Table 3. Step 7 Point System

Value		Points
<i>Mass Flux ($\rho V_p / \sigma_{\rho V_p}$)</i>		
>4.5		5
>4.0		3
>3.5		2
>3.0		1
<i>Tangential Momentum Flux/$\sigma_{\text{Tang.Mom.}}$</i>		
>1.5		5
>1.0		3
>0.7		2
>0.5		1
<i>Alfvén Mach Number ($M_A - \sigma_{M_A}$)</i>		
>4.2		10
>3.4		9
>3.0		7
>2.5		6
>2.2		2
>1.5		1
<i>Velocity (V_S / σ_{V_S})</i>		
>14		15
>13		13
>12		10
>10		9
>9		4
<i>Velocity Deviation</i>		
<35		10
<40		8
<45		6
<50		3
<60		2
<i>Θ_{Bn} Uncertainty (σ_{Bn})</i>		
<1.7		10
<1.9		8
<2.3		6
<4.0		3
<i>Density Compression Ratio ($R_N - \sigma_{R_N}$)</i>		
>2.9		20
>2.6		17
>2.4		14
>2.1		10
>2.0		5
>1.5		2
<i>Magnetic Compression Ratio ($R_B - \sigma_{R_B}$)</i>		
>1.9		25
>1.5		18
>1.4		13
>1.3		10
>1.1		5
>1.0		2

changes in the program and is subject to optimization. (Table 4).

5. Discussion

[35] Table 5 offers a year-by-year breakdown of the performance of the automated analysis operating on the ACE Level-2 data over the extended period 1999 through 2005 through step 6. Shocks identified for 2004 and 2005

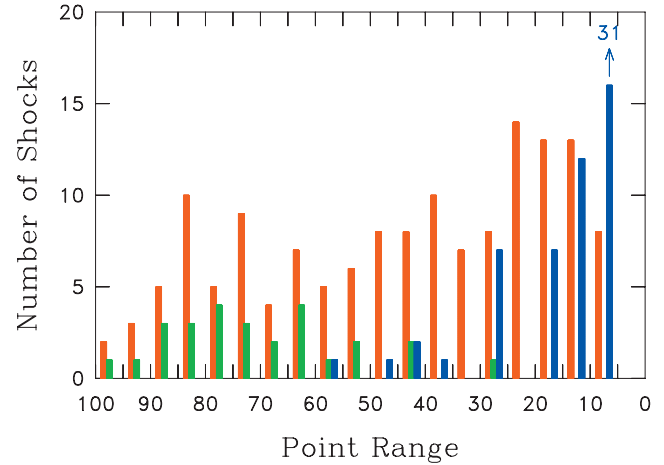


Figure 7. Computed point value according to Table 3 for each shock found by the automated analysis from late 1998 through early 2005. Red represents all true shocks, green shows strong shocks (either $M_A > 3$, $R_N > 3$, or $R_B > 3$), and blue represents false shock solutions passed by the analysis through step 6. Number of false shock solutions with point values between 5 and 10 is off scale at 31.

are at this time only candidates awaiting validation by the ACE team. These numbers are likely to change. In the latter years there are very few interactive solutions at this time. Interactive solutions take time and time is money. One application of this automated analysis is to increase the library of shock solutions in a quick and relatively cheap manner. Not only is it possible to adopt the solutions described on this table once they have been examined further, but the selection and rejection conditions can be eased to admit a greater number of true weak shocks while allowing more false positive shocks to pass the analysis. For analyses not running in a space weather environment, this is perfectly acceptable. Then the shock times can be compared to those identified by the user and the validity of real shocks judged not by the automated code, but by the operator after the fact. This will permit us to rapidly extend the shock solution data base retroactively in a reliable and inexpensive manner for the purpose of doing science with the science-quality data. Other spacecraft teams are welcome to use the code in this same manner.

[36] Some low M_A and marginally supercritical shocks not previously recognized by the ACE team have been

Table 4. Comparison of Solutions

	$\langle I_i - A_i \rangle$	$\langle I_i - A_i \rangle^{M_A > 3}$
V_P	31.3 km/s	45.5 km/s
V_S	78.9 km/s	72.2 km/s
M_A	0.53	1.05
R_n	0.19	0.27
R_b	0.25	0.25
Θ_{Bn}	8.8°	9.1°

Table 5. Yearly Comparison of Solutions

Years Analyzed	Total Number of Shocks	Interactive Analysis	Shocksolver Step 1	Shocksolver Step 2	Shocksolver Step 6	Both Interactive and Automated Solutions
1999–2005	344	171	248	223	143	105
1999	43	33	34	33	24	23
2000	68	51	54	49	31	30
2001	75	46	48	40	28	28
2002	57	33	41	39	19	17
2003	54	8	38	34	17	7
2004	25	0	18	16	13	0
2005	22	0	15	12	11	0

found and analyzed using this same algorithm. These shocks are often characterized by the slow rise in proton temperature downstream of (behind) the shock [Whang *et al.*, 1998; Liu *et al.*, 2007; and references therein] and were previously thought to be ‘wavelike’ behavior in the data. These events were originally rejected from the shock list. A list of such solutions is now being developed for further study.

6. Summary

[37] We have converted a code previously written to solve the Rankine-Hugoniot shock equations interactively [Szabo, 1994] and made it run in an automated, hands-off environment suitable for space weather studies. In so doing we have developed a program that finds suitable shock candidates in spacecraft data containing both thermal proton and magnetic field data and then refines that event list based on local measurements (± 10 min of the shock candidate time). The preexisting code (shock normal and asymptotic magnetofluid calculations) was made to run in a more robust, noninteractive form at the expense of sometimes missing a solution. The resulting automated solutions are then used to assess the quality of the shock candidate and to reject events with statistically insignificant conserved quantities. The use of the shock solution in this way is a major aspect of the new method.

[38] Running the fully automated code on science-quality data from the ACE spacecraft, we find two fifths of all previously identified shocks including many shocks too weak for significant space weather application and two thirds of all shocks with previous interactive solutions (those shocks of most relevance to space weather and particle acceleration science). In the case of the strongest shocks, only four shocks with either $M_A > 3$, $R_N > 3$, or $R_B > 3$ were missed by the fully automated analysis. Additionally, the code passes as real 31 false positive identifications in the years 1999–2002 and 62 false shocks in the years 1999–2005, none of which possess solutions in the strong shock range. Only three strong shocks were missed in the years 1999–2002. However, the ACE team has yet to review the later years and some shock candidates listed for 2003 to the present may be removed from the list and others added. This is accomplished by tests that require a statistically significant shock solution with finite shock speed, mass flux,

and tangential momentum greater than their computed uncertainties. We have shown that a final filtering scheme based on a greater range of shock conditions can be constructed to eliminate all false positive shock events at the expense of losing some additional weak shocks and six strong shock event. This last step is easily tuned to admit more real shocks at the expense of occasionally admitting false shock events. Future improvement of the technique must involve not so much the ability to determine good events at the end of the analysis; rather it must focus on the difficulty of finding shock events in otherwise disturbed data intervals. Comparison of shock parameters computed for the automated and interactive solutions shows a consistent 1σ deviation, meaning that automated and interactive solutions are statistically equivalent in most cases. Comparison of strong shocks found by both the automated and interactive analyses likewise show good agreement in their solutions at about the 1σ level.

[39] An alternative shock selection mechanism based purely on the shock point system finds 78 real shocks, of which 28 are strong, in the 1998–2005 data set, while accepting only six false positives from the years 2004–2005. These solutions await confirmation and the false positives could in fact be recognized as real shocks. The point system can be easily modified with simple changes in the program and is subject to optimization.

[40] **Acknowledgments.** The authors thank M. K. Hudson, H. Kucharek, J. Raeder, and M. F. Thomsen for helpful discussions. Funding for this work was provided by NASA grants NNG04GMO5G, NAG5-12492, and Caltech subcontract 44A-1062037 in support of the ACE/MAG experiment. Support at LANL was provided under the auspices of the U. S. Department of Energy, with financial support from the NASA ACE program. V. S. Vorotnikov is an undergraduate Junior pursuing a major in renewable energy technology at the University of New Hampshire.

References

- Armstrong, T. P., M. E. Pesses, and R. B. Decker (1985), Shock drift acceleration, in *Collisionless Shocks in the Heliosphere: Reviews of Current Research, Geophys. Monogr. Ser.*, vol. 35, edited by B. T. Tsurutani, and R. G. Stone, pp. 271–285, AGU, Washington, D. C.
- Berdichevsky, D. B., A. Szabo, R. P. Lepping, A. F. Viñas, and F. Mariani (2000), Interplanetary fast shocks and associated drivers

- observed through the 23rd solar minimum by Wind over its first 2.5 years, *J. Geophys. Res.*, **105**, 27,289–27,314.
- Boyd, T. J., and J. J. Sanderson (1969), *Plasma Dynamics*, Barnes and Noble, New York.
- Burlaga, L. F. (1995), *Interplanetary Magnetohydrodynamics*, Oxford Univ. Press, New York.
- Desai, M. I., G. M. Mason, J. R. Dwyer, J. E. Mazur, R. E. Gold, S. M. Krimigis, R. M. Skoug, and C. W. Smith (2003), Evidence for a suprathermal seed population of heavy ions accelerated by interplanetary shocks near 1 AU, *Astrophys. J.*, **588**, 1149–1162.
- Dryer, M., Z. Smith, C. D. Fry, W. Sun, C. S. Deehr, and S.-I. Akasofu (2004), Real-time shock arrival predictions during the “Halloween 2003 epoch,” *Space Weather*, **2**, S09001, doi:10.1029/2004SW000087.
- Echer, E., and W. D. Gonzalez (2004), Geoeffectiveness of interplanetary shocks, magnetic clouds, sector boundary crossings and their combined occurrence, *Geophys. Res. Lett.*, **31**, L09808, doi:10.1029/2003GL019199.
- Echer, E., W. D. Gonzalez, and M. V. Alves (2006), On the geomagnetic effects of solar wind interplanetary magnetic structures, *Space Weather*, **4**, S06001, doi:10.1029/2005SW000200.
- Farrugia, C. J., V. K. Jordanova, M. F. Thomsen, G. Lu, S. W. H. Cowley, and K. W. Ogilvie (2006), A two-ejecta event associated with a two-step geomagnetic storm, *J. Geophys. Res.*, **111**, A11104, doi:10.1029/2006JA011893.
- Forman, M. A., and G. M. Webb (1985), Acceleration of energetic particles, in *Collisionless Shocks in the Heliosphere: A Tutorial Review*, *Geophys. Monogr. Ser.*, vol. 35, edited by R. G. Stone and B. T. Tsurutani, pp. 91–114, AGU, Washington, D. C.
- Giacalone, J. (2005), Particle acceleration at shocks moving through an irregular magnetic field, *Astrophys. J.*, **624**, 765–772.
- Gonzalez, W. D., B. T. Tsurutani, and A. L. Clu’ a de Gonzalez (1999), Interplanetary origin of geomagnetic storms, *Space Sci. Rev.*, **88**, 529–562.
- Gosling, J. T., and D. J. McComas (1987), Field line draping about fast coronal mass ejecta: A source of strong out-of-the-ecliptic interplanetary magnetic fields, *Geophys. Res. Lett.*, **14**, 355–358.
- Gosling, J. T., and V. J. Pizzo (1999), Formation and evolution of corotating interaction regions and their three dimensional structure, *Space Sci. Rev.*, **89**, 21–52.
- Hudson, M. K., A. D. Kotelnikov, X. Li, I. Roth, M. Temerin, J. Wygant, J. B. Blake, and M. S. Gussenhoven (1995), Simulation of proton radiation belt formation during the March 24, 1991 SSC, *Geophys. Res. Lett.*, **22**(3), 291–294.
- Hudson, M. K., S. R. Elkington, J. G. Lyon, V. A. Marchenko, I. Roth, M. Temerin, J. B. Blake, M. S. Gussenhoven, and J. Wygant (1997), Simulation of radiation belt formation during storm sudden commencements, *J. Geophys. Res.*, **102**(7), 14,087–14,102.
- Jokipii, J. R. (1987), Rate of energy gain and maximum energy in diffusive shock acceleration, *Astrophys. J.*, **313**, 842–846.
- Kallenrode, M.-B. (2001), *Space Physics*, Springer, New York.
- Kappenman, J. G. (2005), An overview of the impulsive geomagnetic field disturbances and power grid impacts associated with the violent Sun-Earth connection events of 29–31 October 2003 and a comparative evaluation with other contemporary storms, *Space Weather*, **3**, S08C01, doi:10.1029/2004SW000128.
- Kress, B. T., M. K. Hudson, and P. L. Slocum (2005), Impulsive solar energetic ion trapping in the magnetosphere during geomagnetic storms, *Geophys. Res. Lett.*, **32**, L06108, doi:10.1029/2005GL022373.
- Lee, M. A. (1984), Particle acceleration and MHD wave excitation upstream of interplanetary shocks, *Adv. Space Res.*, **4**, 295–304.
- Liu, Y. C.-M., M. A. Lee, H. Kucharek, and B. Miao (2007), Ion hermalization and wave excitation downstream of Earth’s bow shock: A theory for Cluster observations of He²⁺ acceleration, *J. Geophys. Res.*, **112**, A07217, doi:10.1029/2006JA012239.
- McComas, D. J., et al. (1998), Solar wind electron proton alpha monitor (SWEPAM) for the Advanced Composition Explorer, *Space Science Rev.*, **86**(1–4), 563–612.
- McKenna-Lawlor, S. M. P., M. Dryer, M. D. Kartalev, Z. Smith, C. D. Fry, W. Sun, C. S. Deehr, K. Kecskemety, and K. Kudela (2006), Near real-time predictions of the arrival at Earth of flare-related shocks during Solar Cycle 23, *J. Geophys. Res.*, **111**, A11103, doi:10.1029/2005JA011162.
- Neugebauer, M., and J. Giacalone (2005), Multispacecraft observations of interplanetary shocks: Nonplanarity and energetic particles, *J. Geophys. Res.*, **110**, A12106, doi:10.1029/2005JA011380.
- Neugebauer, M., J. Giacalone, E. Chollet, and D. Lario (2006), Variability of low-energy ion flux profiles on interplanetary shock fronts, *J. Geophys. Res.*, **111**, A12107, doi:10.1029/2006JA011832.
- Posner, A. (2007), Up to 1-hour forecasting of radiation hazards from solar energetic ion events with relativistic electrons, *Space Weather*, **5**, S05001, doi:10.1029/2006SW000268.
- Siscoe, G., P. J. MacNeice, and D. Odstrcil (2007), East-west asymmetry in coronal mass ejection globe geoeffectiveness, *Space Weather*, **5**, S04002, doi:10.1029/2006SW000286.
- Smith, C. W., M. H. Acuña, L. F. Burlaga, J. L’Heureux, N. F. Ness, and J. Scheifele (1998), The ACE magnetic field experiment, *Space Sci. Rev.*, **86**(1–4), 613–632.
- Stone, E. C., A. M. Frandsen, R. A. Mewaldt, E. R. Christian, D. Margolis, J. F. Ormes, and F. Snow (1998), The Advanced Composition Explorer, *Space Sci. Rev.*, **86**(1–4), 1–22.
- Szabo, A. (1994), An improved solution to the “Rankine-Hugoniot” problem, *J. Geophys. Res.*, **99**, 14,737–14,746.
- Thomsen, M. F. (1985), Upstream suprathermal ions, in *Collisionless Shocks in the Heliosphere: Reviews of Current Research*, *Geophys. Monogr. Ser.*, vol. 35, edited by B. T. Tsurutani and R. G. Stone, pp. 253–270, AGU, Washington, D. C.
- Tóth, G., D. L. De Zeeuw, T. I. Gombosi, W. B. Manchester, A. J. Ridley, I. V. Sokolov, and I. I. Roussev (2007), Sun-to-thermosphere simulation of the 28–30 October 2003 storm with the Space Weather Modeling Framework, *Space Weather*, **5**, S06003, doi:10.1029/2006SW000272.
- Trichtchenko, L., A. Zhukov, R. van der Linden, S. M. Stankov, N. Jakowski, I. Stanisawska, G. Juchnikowski, P. Wilkinson, G. Patterson, and A. W. P. Thomson (2007), November 2004 space weather events: Real-time observations and forecasts, *Space Weather*, **5**, S06001, doi:10.1029/2006SW000281.
- Vandegriff, J., K. Wagstaff, G. Ho, and J. Plauger (2005), Forecasting space weather: Predicting interplanetary shocks using neural networks, *Adv. Space Res.*, **36**, 2323–2327.
- Viñas, A. F., and J. D. Scudder (1986), Fast and optimal solution to the ‘Rankine-Hugoniot problem’, *J. Geophys. Res.*, **91**, 39–58.
- Webb, D. F. (2004), Coronal mass ejections and space weather, in *Multi-Wavelength Investigations of Solar Activity*, *Proc. IAU Symp.*, vol. 223, edited by A. V. Stepanov, E. E. Benevolenskaya, and A. G. Kosovichev, pp. 499–508, Int. Astron. Union, Paris.
- Whang, Y. C., D. Larson, R. P. Lin, R. P. Lepping, and A. Szabo (1998), Plasma and magnetic field structure of a slow shock: Wind observations in interplanetary space, *Geophys. Res. Lett.*, **25**, 2625–2628.
- Xie, H., N. Gopalswamy, L. Ofman, O. C. St. Cyr, G. Michalek, A. Lara, and S. Yashiro (2006), Improved input to the empirical coronal mass ejection (CME) driven shock arrival model from CME cone models, *Space Weather*, **4**, S10002, doi:10.1029/2006SW000227.
- Zwicky, R. D., et al. (1999), The NOAA Real-Time Solar-Wind (RTSW) System using ACE Data, *Space Sci. Rev.*, **86**(1–4), 633–648.
- C. M. S. Cohen, Space Radiation Laboratory, California Institute of Technology, MC 220-47, 1200 East California Avenue, Pasadena, CA 91125, USA. (cohen@srl.caltech.edu)
- Q. Hu, Institute of Geophysics and Planetary Physics, University of California, Riverside, Riverside, CA 92521, USA. (qiang.hu@ucr.edu)
- R. M. Skoug, Los Alamos National Laboratory, MS D466, Los Alamos, NM 87545, USA. (rskoug@lanl.gov)
- C. W. Smith, Space Science Center, University of New Hampshire, Morse Hall, Durham, NH 03824, USA. (charles.smith@unh.edu)
- A. Szabo, NASA Goddard Space Flight Center, Code 672, Greenbelt, MD 20771, USA. (adam.szabo@nasa.gov)
- V. S. Vorotnikov, Department of Chemical Engineering, University of New Hampshire, Durham, NH 03824, USA. (vsn3@unh.edu)